Stacking-faults-free zinc blende GaAs/AlGaAs axial heterostructure nanowires during vapor-liquid-solid growth

Jingwei Guo (郭经纬)*, Hui Huang (黄 辉), Xiaomin Ren (任晓敏), Xin Yan (颜 鑫), Shiwei Cai (蔡世伟), Yongqing Huang (黄永清), Qi Wang (王 琦), Xia Zhang (张 霞), and Wei Wang (王 伟)

Key Laboratory of Information Photonics and Optical Communications, Ministry of Education, Beijing University of Posts and Telecommunications, Beijing 100876, China

**Corresponding author: guojingwei666@163.com*

Received September 27, 2010; accepted December 7, 2010; posted online March 15, 2011

Pure zinc blende structure GaAs/AlGaAs axial heterostructure nanowires (NWs) are grown by metal organic chemical vapor deposition on GaAs(111) B substrates using Au-catalyzed vapor-liquid-solid mechanism. Al adatom enhances the influence of diameters on NWs growth rate. NWs are grown mainly through the contributions from the direct impingement of the precursors onto the alloy droplets and not so much from adatom diffusion. The results indicate that the droplet acts as a catalyst rather than an adatom collector.

OCIS codes: 160.4236, 310.3840.
doi: 10.3788/COL201109.041601.

In the past few years, semiconductor nanowires (NWs) have attracted a great deal of interest due to their potential applications in electronic and optoelectronic devices[1,2]. The Au-catalyzed vapor-liquid-solid (VLS) mechanism is a commonly used method for semiconductor NW growth[3,4]. At growth temperature, Au nanoparticles (NPs) on the substrate surface form alloy droplets with the group III growth precursor(s). Semiconductor NWs are grown from supersaturated alloy droplets.

GaAs/AlGaAs heterostructure NWs are one of the most popular NWs. GaAs and AlGaAs have almost the same lattice constant, and the difference between their band gaps and refractive indices is large, which is advantageous for applications in optoelectronic devices[5,6]. However, many studies have focused on the GaAs/AlGaAs radial heterostructure[7−13], which is a core-shell structure, and little research has been conducted on the GaAs/AlGaAs axial heterostructure. In this letter, the growth of Au-assisted GaAs/AlGaAs axial heterostructure NWs is investigated, and the related growth mechanism is discussed.

The growth was performed in a Thomas Swan close coupled showerhead metal-organic chemical vapor deposition (CCS-MOCVD) system at a pressure of 100 torr. Trimethylgallium (TMGa, 4×10^{-5} mol/min) and AsH_3 (2.8×10^{-3} mol/min) were precursors for GaAs growth. When AlGaAs was grown, trimethylaluminum (TMAl, 4×10^{-5} mol/min) was introduced with the same TMGa and AsH_3 flows. The carrier gas was hydrogen.

Prior to growth initiation, an Au film with a thickness of 4 nm was deposited on the GaAs (111) B substrate by magnetron sputtering. The Au-coated substrate was then loaded into the MOCVD reactor and annealed *in situ* at 650 °C in arsine and hydrogen ambient for the desorption of surface contaminants and the formation of alloy droplets as catalyst. After ramping down to the growth temperature, GaAs NWs were firstly grown for 600 s at 440 °C, which is the optimum temperature based on a number of experiments (at a lower temperature NWs will be kinked; at a higher temperature, taper will occur). Five pairs of AlGaAs (10 s)/GaAs (10 s) heterostructure junctions were grown at the same temperature.

The morphologies of as-grown NWs were studied using a HITACHI S-5500 field-emission scanning electron microscope (SEM). The structure and chemical compositions of a single NW were characterized using an FEI TECNAI F30 field-emission transmission electron microscope (TEM) equipped with energy dispersive X-ray spectroscopy (EDS) as well as a scanning transmission electron microscope (STEM). For the preparation of TEM samples, the NWs were removed from the substrate by sonication into ethanol suspension for 2 min. A small volume of the NW suspension was left to dry onto a holey carbon film supported by a Cu mesh TEM grid.

Cross-sectional views of the SEM images of the grown NWs are shown in Fig. 1. All NWs are vertical to the substrate. There are five junctions in each NW because of the changes in the volume of the alloy droplets at the tip of the NWs caused by different supersaturations of Ga and Al dissolved in Au NPs. The supersaturation of

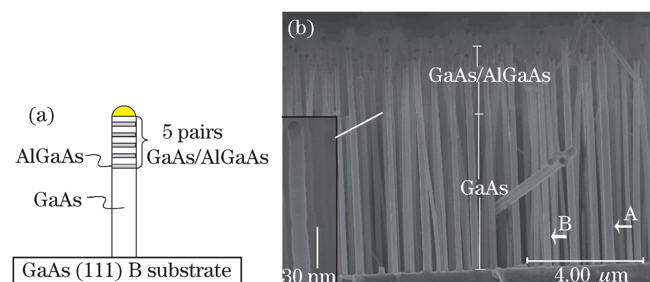

Fig. 1. (a) Sketch of the proposed NW configuration; (b) cross-section view of the SEM image of GaAs/AlGaAs NWs. The inset is a magnified pattern of the top segment of one NW.

 © 2011 Chinese Optics Letters

Al is smaller than that of Ga; thus, the segments with smaller diameters are AlGaAs sections.

The length of NWs slightly depends on the diameter. As shown in Fig. 1(b), the length of the NW with a diameter of 313 nm is 8.23 μm (as indicated by arrow A); however, the length of the NW with a diameter of 201 nm is 7.1 μm (as indicated by arrow B). Previously, we reported that the growth rate of GaAs NWs is diameter independent[14]. Thus, Al adatom can be concluded to enhance the influence of the diameter on the growth rate of NWs. NWs with a larger diameter grow faster than those with a smaller diameter. The Givargizov-Chernov theory provides the following expression between the length (L) and the radius (R) of NWs[15]:

$$L = K\left[\Delta\mu_{\rm v}^{0} - \frac{2\Omega_{\rm s}\gamma_{\rm sv}}{k_{\rm B}TR}\right]^2 t, \quad (1)$$

where $\Delta\mu_{\rm v}^{0}$ is the difference of the chemical potentials of atoms in the vapor and solid phases (in $k_{\rm B}T$ units, T is the substrate temperature during NW growth, and $k_{\rm B}$ is the Boltzmann constant) for the planar interfacial boundary, $\gamma_{\rm sv}$ is the surface energy of the solid-vapor boundary (per unit area), $\Omega_{\rm s}$ is the volume per atom in the crystal, K is an unknown coefficient of crystallization from the alloy droplet, and t is the growth time. The second term in the square brackets on the right-hand side of Eq. (1) arises due to the curvature of the NW surface. Equation (1) qualitatively explains the increase in the NW length with an increase in diameter at a given growth time. The experimental data and corresponding line calculated by Eq. (1) are shown in Fig. 2. However, when the diameter of NWs is larger than 300 nm, there is a large misfit between Eq. (1) and the experimental data. Equation (1) should be revised for NWs with a larger diameter (>300 nm).

Based on the top view SEM image, as shown in Fig. 3, the NW shape is hexagon, and the sidewall facets belong to {112} families of planes, similar to the findings in Refs. [16,17]. These results are different from those reported in Refs. [9,12], whose facets are {110} families of planes. The {112} facets have a larger number of surface dangling bonds with respect to the {110} facets that tend to reconstruct (Ga-Ga and As-As dimers)[18]. This may lower the surface energy of {112} facets to less than that of {110} facets.

The VLS growth has two major contributions: direct

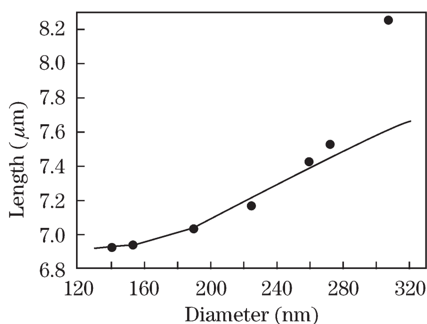

Fig. 2. Dependence of the NW length on the diameter. Dots represent experimental data; line represents the results of the calculations by Eq. (1).

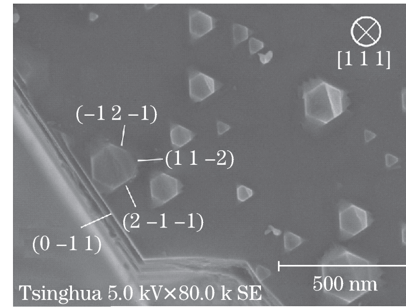

Fig. 3. Top view of the SEM image of NWs.

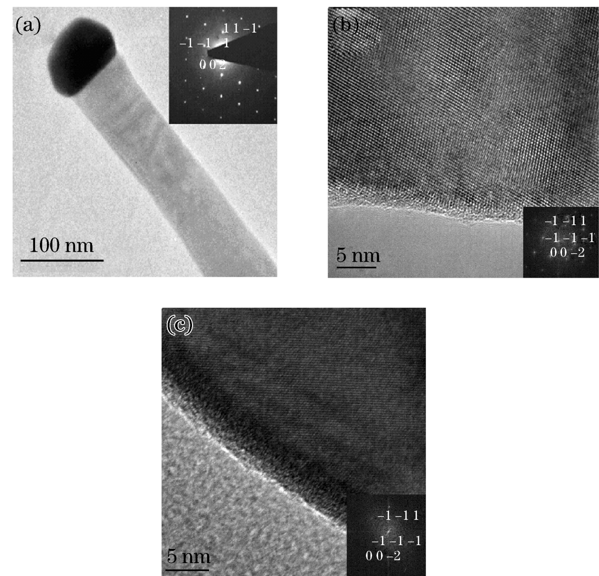

Fig. 4. TEM analyses of a NW with a diameter of 81 nm. (a) Bright field TEM image of the NW with an alloy particle at the tip (the corresponding SAED is shown as an inset); (b) HRTEM image of the middle section of the NW; (c) HRTEM image of the bottom section of the NW. In (b) and (c), the corresponding Fourier transform of the structure is shown as an inset.

impingement of the precursors onto the alloy droplet and adatom diffusion from the sidewalls and substrate surface to the top[19−21]. The adatom diffusion has been demonstrated to result in lateral overgrowth and tapering when the wire length is longer than the diffusion length of the adatom, and the growth rate is inversely dependent on the diameter[22−24]. In our case, as shown in Fig. 1(b), a remarkable phenomenon was observed: lateral overgrowth and tapering of the NWs did not occur because the NWs had a constant diameter from base to top. Thus, in our case, the NWs can be concluded to have grown with negligible contribution from adatom diffusion and with major contribution from the catalytic pyrolysis of the precursors impinging onto the alloy droplet. In other words, the droplet acts as a catalyst rather than a collector of adatom.

TEM and high resolution TEM (HRTEM) images of the NW with a diameter of 81 nm are presented in Fig. 4. These images were taken with [1−10] direction of the electron beam incidence. As shown in Fig. 4(a), the selected area electron diffraction (SAED) indicates a pure

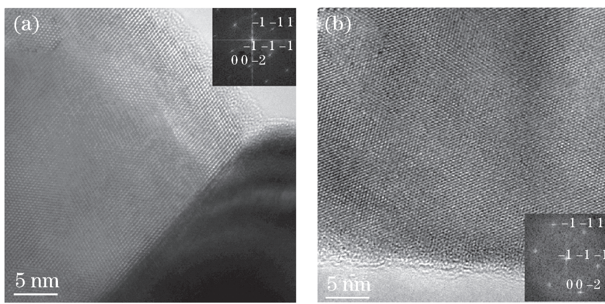

Fig. 5. TEM analyses of a wire with a diameter of 114 nm. (a) HRTEM image of the alloy particle capped NW tip; (b) HRTEM image of the middle section of the NW. The corresponding Fourier transform of the structure is shown as an inset.

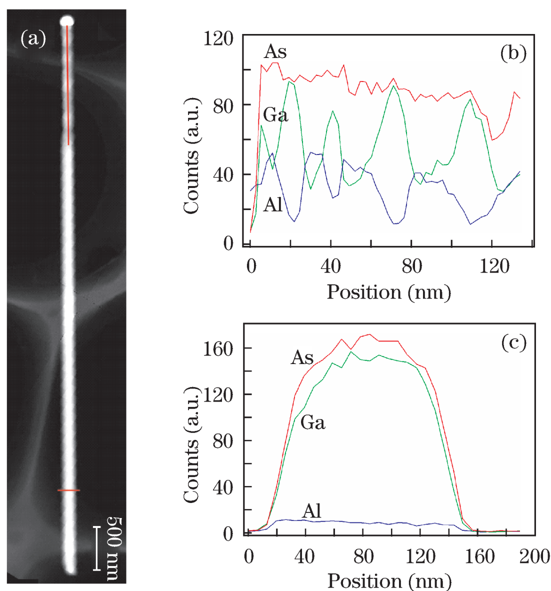

Fig. 6. (a) Dark field STEM image of one NW; (b) Corresponding EDS image of the top vertical line; (c) Corresponding EDS image of the bottom horizontal line.

zinc blende structure, and no stacking fault is observed in the NWs. HRTEM images of the middle and bottom sections of the NW are shown in Figs. 4(b) and (c), respectively. These images and the corresponding Fourier transform confirm the pure zinc blende structure of the NW.

Figure 5 shows the TEM analyses of a NW with a diameter of 114 nm. The TEM images were taken with [1−1 0] direction of the electron beam incidence. HRTEM images of the top and middle sections of the NW with the corresponding Fourier transform are shown in Figs. 5(a) and (b), respectively. The structure is a pure zinc blende structure of the NW, and no stacking fault is observed.

The growth conditions of NWs, such as the high growth rate and the relatively high V/III ratio, may all contribute to the reduction of the planar defects, such as stacking faults and twins, in the NWs[25]. Moreover, fluctuations in the composition and size of the droplet also result in stacking faults or twins in the NW due to the change in tension and supersaturation in the droplet[26,27]. Fluctuations in composition and size of the droplet can be induced by the Ga and Al adatom diffusion from the sidewall and substrate surface because the amount of adatom diffusing into the droplet varies with the lateral overgrowth as well as with the NW length. However, GaAs and AlGaAs have almost the same lattice constant, and there is no tension at their interface. Thus, the droplet remains stable during growth with negligible contribution from the Ga and Al adatom diffusion, which also contributes to the growth of stacking-fault-free NWs.

EDS measurements were performed to probe the elemental distribution along the length and the diameter of the NWs. The EDS images of the top and bottom sections of one NW are shown in Fig. 6. The lines in the NWs are scan lines. As shown in Fig. 6(b), the Al and Ga counts reveal five periods where the Al and Ga signal variations are anticorrelated. The regions with higher Al signal and corresponding lower Ga signal are indicative of the presence of the AlGaAs segment. In Fig. 6(c), the Al signal is weak along the diameter of the NW. Very thin growth of AlGaAs shells on the NWs surface was confirmed. This result can be ascribed to the low-temperature growth. Thick shells can only be grown at a high temperature[7−13]. Based on the EDS analyses, heterostructure junctions were axially grown along the ⟨111⟩ direction.

In conclusion, vertical GaAs/AlGaAs axial heterostructure NWs are grown on GaAs (111) B substrate using the VLS mechanism. The high growth rate, the relatively high V/III ratio, and the same lattice constant between GaAs and AlGaAs contribute to the growth of stacking-fault-free NWs. Moreover, NWs are grown mainly through the contributions from the direct impingement of the precursors onto the alloy droplets and not so much from the contributions from adatom diffusion. The results indicate that the droplet acts as a catalyst rather than an adatom collector.

This work was supported by the National Basic Research Program of China (No. 2010CB327600), the National High Technology R&D Program of China (No. 2009AA03Z417), the National Natural Science Foundation of China (No. 61020106007), the Program for New Century Excellent Talents in University of Ministry of Education of China (NCET-08-0736), the Chinese Universities' Scientific Fund (BUPT2009RC0409, BUPT2009RC0410), and the 111 Program of China (No. B07005).

References

1. F. Patolsky, B. P. Timko, G. Yu, Y. Fang, A. B. Greytak, G. Zheng, and C. M. Lieber, Science **313,** 1100 (2006).
2. T. Bryllert, L.-E. Wernersson, L. E. Fröberg, and L. Samuelson, IEEE Electron Device Lett. **27,** 323 (2006).
3. R. S. Wagner and W. C. Ellis, Appl. Phys. Lett. **4,** 89 (1964).
4. H. Huang, X. Ren, X. Ye, J. Guo, Q. Wang, Y. Yang, S. Cai, and Y. Huang, Nano Lett. **10,** 64 (2010).
5. Y. Yao, T. Ochiai, T. Mano, T. Kuroda, T. Noda, N. Koguchi, and K. Sakoda, Chin. Opt. Lett. **7,** 882 (2009).
6. X. Mi, D. Li, F. Meng, and H. Zhao, Chin. Opt. Lett. **7,** 335 (2009).
7. C. Chen, N. Braidy, C. Couteau, C. Fradin, G. Weihs,

and R. LaPierre, Nano Lett. **8,** 495 (2008).

8. Z. H. Wu, M. Sun, X. Y. Mei, and H. E. Ruda, Appl. Phys. Lett. **85,** 657 (2004).
9. M. J. Tambe, S. K. Lim, M. J. Smith, L. F. Allard, and S. Gradečak, Appl. Phys. Lett. **93,** 151917 (2008).
10. K. Tateno, H. Gotoh, and Y. Watanabe, Appl. Phys. Lett. **85,** 1808 (2004).
11. L. Ouattara, A. Mikkelsen, N. Sköld, J. Eriksson, T. Knaapen, E. Ćavar, W. Seifert, L. Samuelson, and E. Lundgren, Nano Lett. **7,** 2859 (2007).
12. J. Noborisaka, J. Motohisa, S. Hara, and T. Fukui, Appl. Phys. Lett. **87,** 093109 (2005).
13. K. Tomioka, Y. Kobayashi, J. Motohisa, S. Hara, and T. Fukui, Nanotechnology **20,** 145302 (2009).
14. X. Ye, H. Huang, X.-M. Ren, Y.-S. Yang, J.-W. Guo, Y.-Q. Huang, and Q. Wang, Chin. Phys. Lett. **27,** 046101 (2010).
15. V. G. Dubrovskii and N. V. Sibirev, Phys. Rev. E **70,** 031604 (2004).
16. M. Moewe, L. C. Chuang, S. Crankshaw, C. Chase, and C. Chang-Hasnain, Appl. Phys. Lett. **93,** 023116 (2008).
17. B. A. Wacaser, K. Deppert, L. S. Karlsson, L. Samuelson, and W. Seifert, J. Cryst. Growth **287,** 504 (2006).
18. R. Magri, M. Rosini, and F. Casetta, Phys. Stat. Sol. C **7,** 374 (2010).
19. C. Soci, X.-Y. Bao, D. P. R. Aplin, and D. Wang, Nano Lett. **8,** 4275 (2008).
20. M. C. Plante and R. R. LaPierre, J. Cryst. Growth **310,** 356 (2008).
21. V. G. Dubrovskii, N. V. Sibirev, G. E. Cirlin, I. P. Soshnikov, W. H. Chen, R. Larde, E. Cadel, P. Pareige, T. Xu, B. Grandidier, J.-P. Nys, D. Stievenard, M. Moewe, L. C. Chuang, and C. Chang-Hasnain, Phys. Rev. B **79,** 205316 (2009).
22. V. G. Dubrovskii, N. V. Sibirev, G. E. Cirlin, M. Tchernycheva, J. C. Harmand, and V. M. Ustinov, Phys. Rev. E **77,** 031606 (2008).
23. J. C. Harmand, G. Patriarche, N. Péré-Laperne, M-N. Mérat-Combe, L. Travers, and F. Glas, Appl. Phys. Lett. **87,** 203101 (2005).
24. A. I. Persson, B. J. Ohlsson, S. Jeppesen, and L. Samuelson, J. Cryst. Growth **272,** 167 (2004).
25. H. J. Joyce, Q. Gao, H. H. Tan, C. Jagadish, Y. Kim, X. Zhang, Y. Guo, and J. Zou, Nano Lett. **7,** 921 (2007,).
26. J. Bauer, V. Gottschalch, H. Paetzelt, G. Wagner, B. Fuhrmann, and H. S. Leipner, J. Cryst. Growth **298,** 625 (2007).
27. F. Glas, J.-C. Harmand, and G. Patriarche, Phys. Rev. Lett. **99,** 146101 (2007).